DOI: 10.61782/fa.2023.1107

forum acusticum 2023

NUMERICAL AND EXPERIMENTAL CHARACTERIZATION OF AN ISOLATED LOW-REYNOLDS ROTOR IN PUSHER CONFIGURATION

Caterina Poggi[1*] **Elisa de Paola**[1] **Luana G. Stoica**[1] **Alessandro Di Marco**[1]

[1] Department of Civil, Computer Science and Aeronautical Technologies Engineering, RomaTre University, Rome, Italy

ABSTRACT

The present paper proposes a numerical/experimental investigation of the aerodynamics and aeroacoustics of an isolated low-Reynolds rotor. An experimental campaign is carried out to evaluate the flow field downstream of the rotor through PIV measurements, whereas two microphone arrays are adopted to characterize the noise directivity. The numerical analyses are performed by the combined application of a boundary integral formulation suitable for the potential aerodynamics solution around lifting/thrusting bodies and the Farassat 1A formulation for the evaluation of the radiated noise. Several operating conditions are tested. The results demonstrate a good agreement between numerical predictions and experimental measurements sets the basis for the creation of a wide database exploiting the potentiality of both approaches in the perspective of establishing low-cost methods to be used in the preliminary design of complex, innovative solutions.

Keywords: *rotor noise, piv, aeroacoustics, boundary element method.*

1. INTRODUCTION

In recent years, demand for air transport has grown dramatically and is expected to double in the next ten years, [1]. Concerns about the worsening environmental impact and the rising cost of oil due to the pandemic and the international political situation have revived the interest in propeller-driven configuration since efficient propulsion systems are required to achieve a step-change in the performance of future aircraft designs. In this context, industry and the scientific community have shown a great interest in hybrid-electric [2] and fully-electric [3] propulsion. Electric propulsion is expected to modify the classical frequency spectrum of the sound emission, altering the relationships currently used between noise exposure and annoyance. Additionally, the use of UAV (Unmanned Aerial Vehicle) systems is rapidly growing in a wide range of applications, such as surveillance, search and rescue missions, and delivery. A consequence of this fact is the compelling need to identify noise reduction technologies in order to guarantee environmentally sustainable aviation in conformity with the increasingly demanding requirements and certification rules [4]. This results in a growing interest in the investigation of the aerodynamics and aeroacoustic of propellers which represent the primary source of noise for these configurations [5, 6].

The noise emitted by low-Reynolds rotors has been experimentally and numerically investigated in many research studies, focusing on the directivity of the isolated propeller [5] as well as on the effect of the blade geometry and on the rotor-airframe interactions [7, 8]. A different approach was followed by Tinney et al. in [9] to compare the noise due to isolated rotors, quadcopters, and hexacopters operating at static thrust. More recently, work done by Grande et al. [10] experimentally showed the presence of laminar separation bubbles and subsequent broadband noise for a similar sUAS rotor under varying operational conditions. Though those previous studies have uncovered some significant aerodynamic and aeroa-

*__Corresponding author__: *caterina.poggi@uniroma3,it.*

coustic aspects, only a few studies can be found that focus on defining numerical/experimental procedures aimed at developing rapid methods for analyzing single- and multi-rotor configurations.

In order to guarantee a significant reduction of the acoustic nuisance, it is mandatory to include it as a constraint since the early vehicle's design phases. However, this need clashes with the high burden of a reliable aeroacoustic characterization of innovative and complex configurations. For this reason, an alternative low-cost solution to direct costly simulations/tests should be found. In this perspective, a possible solution has been proposed in [11, 12], where computational costly simulations were used to evaluate a numerical database used for metamodels training. Indeed, once trained, surrogate models can be conveniently used as fast tools for the vehicle's design, having the great potential to predict the quantity of interest at the cost of an analytical expression evaluation. The idea at the basis of this work is similar: to set the basis for the creation of a wide database to develop low-cost methodologies, exploiting the potentialities of both numerical and experimental approaches.

As a first step of this research project, a preliminary campaign is performed to investigate the level of agreement between the numerical and the experimental data in terms of aerodynamics and aeroacoustics. To this aim, different operative conditions are examined to better understand their range of variation for which the correlation is still satisfactory. In this paper, the focus is on a single propeller configuration, with the idea that once validated, the proposed methodology can be applied to more complex systems.

The configuration herein investigated is an isolated low-Reynolds propeller, the APC-8x45MR, at static thrust conditions mounted in a pusher position [13]. Both aerodynamics and aeroacoustics are studied numerically and experimentally for several operating conditions, varying the propeller speed within a typical range of applications. The pusher configuration was chosen in that it presents some benefits [14]: i) turbulent high-speed wake does not flow over the nacelle resulting in less drag; ii) the stream tube energizes the flow in front of the propeller, suppressing flow separation on the body; iii) its use results in reduced cabin noise; iv) unobstructed forward view in UAVs and normal force aft of the center of gravity increases the stability.

From an experimental point of view, the aerodynamic investigations are performed through Particle Image Velocimetry (PIV). The acoustic measurements were performed in an anechoic environment using two test set-ups: the first, having the sensors on an arc of circumference in the propeller plane, representing the azimuthal directivity, and the latter, in line and parallel to the propeller axis of rotation, describes the polar directivity. In both cases, the microphones are far enough from the propeller to assume a far-field propagation. The numerical investigations are performed through a boundary integral formulation suitable for the aerodynamics solution of potential-incompressible flows, coupled with the Farassat 1A formulation for the evaluation of the tonal noise contribution. The paper is structured as follows: first, in Sec. 2, the numerical solvers applied are briefly described. Then, in Sec. 3, the experimental procedure is detailed, focusing on the description of both the aerodynamic and aeroacoustic measurements setups, in Sec. 3.1 and in Sec. 3.2, respectively. Finally, in Sec. 4, the numerical/experimental results are reported, and a deep comparison is proposed to highlight the similarities and differences between predictions and how they depend on the operative conditions.

2. NUMERICAL SOLVERS

The numerical investigations are performed through in-house solvers for the solution of the aerodynamic and the acoustic fields, widely validated in the past [15] by comparison against experimental data.

The aerodynamic analysis is performed through a Boundary Element Method (BEM) solver based on the boundary integral formulation introduced in Ref. [16]. Under the assumption of potential and incompressible flows, it is possible to define a potential field, denoted by φ, such that $\boldsymbol{v} = \nabla\varphi$. The potential field is given by the superposition of two contributions: a scattered potential, denoted by φ_S, and an incident one, denoted by φ_I. Sources and doublets distributed over the body surfaces, S_B and doublets distributed over the portion of the wake closer to the trailing edges (the so-called near wakes, indicated as S_W^N), determine the scattered potential. Instead, the incident potential is associated with the doublets distributed over the so-called far wakes S_{W_F} [16], namely the wake region complementary to the near wake. the scattered potential is given by the following integral formulation [16]:

$$\begin{aligned}\varphi_S(\boldsymbol{x},t) = &\int_{S_B}\left[G\left(v_n-u_n\right)-\varphi_S\frac{\partial G}{\partial n}\right]dS(\boldsymbol{y})\\ &-\int_{S_W^N}\Delta\varphi_S\,\frac{\partial G}{\partial n}\,dS(\boldsymbol{y})\end{aligned} \tag{1}$$

where $G = -1/4\pi\, r$ is the unit-source solution of the free-space, three-dimensional Laplace equation, with $r = \|\boldsymbol{y} - \boldsymbol{x}\|$ (namely the distance between observer position, $\boldsymbol{x}$, and source position, $\boldsymbol{y}$); $\Delta\varphi_S$ is the potential jump across the wake surface, known from past history of potential discontinuity at the corresponding body trailing edge through the Kutta condition [17, 18]; $v_n = \boldsymbol{v}_B \cdot \boldsymbol{n}$, where $\boldsymbol{v}_B$ represents the body velocity and $\boldsymbol{n}$ the body outward unit normal, while $u_n = \boldsymbol{u}_I \cdot \boldsymbol{n}$, with $\boldsymbol{u}_I$ denoting the velocity induced by the far wake.

Considering the far wake discretized into M panels, assuming the potential jump constant over each panel, and recalling the equivalence between surface distribution of doublets and vortices, the incident velocity field is evaluated through the Biot-Savart law applied to the vortices having the shape of the panel contours. Furthermore, the Rankine finite-thickness vortex model is applied to guarantee a regular distribution of the induced velocity within the vortex core and thus a more stable algorithm in case of wake-body interactions [16]. Thus, the scattered potential is influenced by the incident potential through the induced velocity, which is then affected by the scattered potential by its trailing-edge discontinuity (which is convected by the wake's material points and defines the intensity of the wake's vortices).

Once the potential field is known, the Bernoulli theorem yields the pressure distribution over the body surface [19], which represents the input for the acoustic analysis. In particular, the acoustic solver is based on the Farassat 1A boundary integral formulation [20] for the solution of the Ffowcs Williams and Hawkings equation. The radiated noise is given by the superposition of two contributions: one depending on the blade geometry and kinematics, the thickness noise, and the other depending on the blade kinematics and the pressure distribution, the loading noise [21].

3. EXPERIMENTAL SETUP AND PROCEDURE

The aerodynamics and aeroacoustics of the different configurations were experimentally analyzed using PIV technique and microphone measurements, whose set-ups are described in the following sections.

3.1 Aerodynamic tests

The flow field velocity immediately downstream of the propeller was measured in the "G. Guj" fluid dynamics laboratory at Roma TRE University through planar 2D PIV measurements. A sketch of the experimental setup is shown in Figure 1. It consists of an Nd:Yag double-pulse laser (200 mJ/pulse at 10 Hz each) and a LaVision SX 4M CCD camera with a resolution of 2360x1776 pixels and a maximum frame rate of 15 Hz, equipped with Nikon lens characterized by a focal length of 50 mm. A Programmable Timing Unit (PTU) provides the trigger signals to synchronize the cross-correlation camera and the Nd-Yag laser to allow the image acquisition. The following Cartesian reference system is adopted: O-XYZ with the origin O in the intersection between the rotor disk and the rotational axis of the propeller chosen as reference. The X-axis is oriented radially and Z-axis is parallel to the axial direction. The air was seeded with smoke particles having a mean diameter of about a few micrometers in order to correctly follow the flow field. A high uniform seeding density in the region of interest was achieved guaranteeing a correct cross-correlation analysis. The PIV image analysis was carried out using the software Davis La Vision. 100 couples of images were acquired at the maximum frequency available from the PIV system to evaluate the instantaneous and averaged flow field.

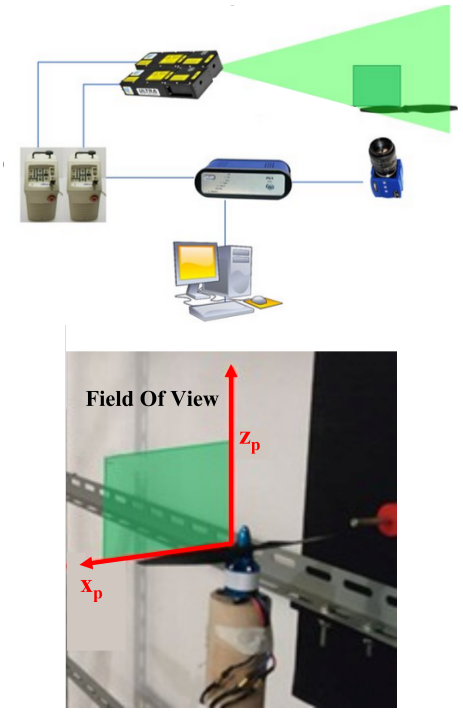

Figure 1. PIV experimental set-up.

3.2 Aeroacoustic tests

The experiments were conducted in the small anechoic chamber "G. Guj" fluid dynamics laboratory at Roma TRE University. The test facility is acoustically treated through wooden-insulated walls covered with sound-absorbent panels (further details are reported in [22, 23]) and measures 3 m in height, 2m in width and 4 m in length. Due to the expected recirculation and turbulence ingestion effects, the flow was facilitated through an outlet and each microphone was shielded with a foam windscreen. A total of seven Microtech Gefell M360 free-field microphones were used to measure the pressure fluctuations from the rotors. The microphone array set-ups for the azimuthal and polar directivity characterization are shown in figures 2 and 3, respectively.

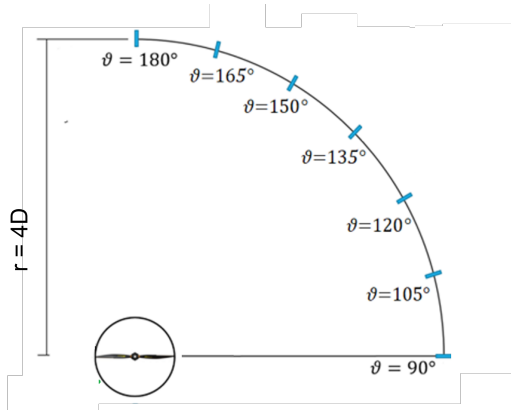

Figure 2. Experimental set-up to characterize the azimuthal directivity.

The circular array was aligned with the plane of the rotors and spanned a range of 90 degrees with a step size of 15°. The linear array was assembled parallel to the test stand. The closest microphone to the rotor in the linear array, and all the sensors in the circular one, were located at a radial distance of 8 rotor radii from the hub center distance, corresponding to the acoustic far-field of the propellers. One more microphone was placed in the nearfield, at a distance not influencing the flow evolution, for the purpose of retrieving and synchronizing the rotational speeds.

The acoustic data were acquired simultaneously for 5 seconds at a sampling rate of 100 kHz, using a NI PXI-6143 data acquisition unit installed on a NI PXIe-8840 chassis.

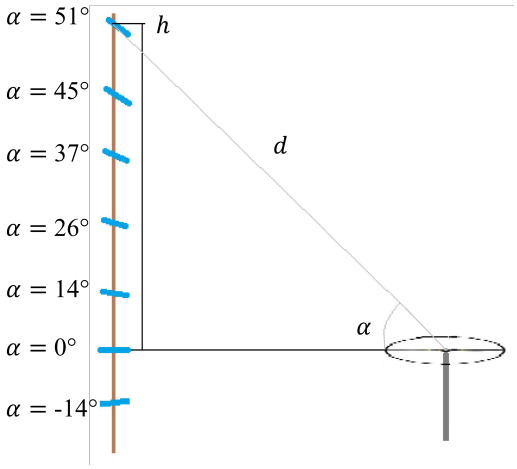

Figure 3. Experimental set-up to characterize the polar directivity.

The acquired data were analyzed in the Fourier domain using the Welch algorithm. The average FFT was calculated on a block of 2^{16} samples for a frequency resolution of 1.5 Hz. A Hanning window and a 50% overlap were applied between each window of the time series.

4. NUMERICAL/EXPERIMENTAL INVESTIGATIONS

The propeller tested is the APC-B8x45MR two-bladed rotor made up of fiberglass composite and characterized by a fixed pitch and a diameter (D) of 203 mm. From the datasheet provided by the manufacturer, the blade geometry is described by the low Reynolds number Eppler E63 airfoil with a Clark-Y similar airfoil near the tip. The rotor was mounted in pusher configuration on a 1.5 D high cylindrical supports made of wood to prevent mechanical vibration and ground effect. A SunnySky X2212 III 1400Kv brushless motor drove the propeller. The rotational rate of the motor is regulated by a FullPower PRO electronic speed controller (ESC), which receives time pulse signals from the digital output of a NI PXI-6143 board. A LabView program was implemented for the open-loop control on the rotational speed, ω. The rotor is tested in hovering condition, at three different angular velocities, 6000 RPM, 7000 RPM, and 8000 RPM.

For the numerical analyses, the geometry of the rotor was reconstructed starting from the blade sectional properties provided by APC. It is important to note that only

the blade geometry is considered in the numerical simulations, whereas the rotor hub is neglected. The results are obtained by discretizing the propeller blades with 35 panels in the chordwise direction and 50 panels in the spanwise direction. The wake surface is discretized by 90000 panels (1800 in the azimuth direction and 50 in the radial direction, distributed along ten revolutions). Furthermore, the aerodynamic computation proceeds in azimuthal steps of 3° and a total of 20 rotor revolutions were computed, whereas, for the acoustic analysis, an azimuthal step of 0.35° is used and the signal recorded for one rotor revolution.

4.1 Aerodynamics

First, a numerical trim analysis is performed to evaluate the blade collective pitch to obtain the same experimental thrust. This is a required preliminary step in that if the same collective pitch of the experimental test is considered, an underestimation of the forces is numerically observed. The results of this analysis are reported in Tab. 1, which shows the target thrust [24] and the additional collective pitch that guarantees the match between the numerical and the experimental thrust with a maximum error of 0.1 N.

Table 1. Trim conditions

RPM	Thrust [N]	Pitch [rad]
6000	2.8	0.096
7000	3.7	0.082
8000	4.9	0.088

Once the collective blade pitch is evaluated, the aerodynamic solver is applied to evaluate the flow-field to be compared with the experimental PIV measurements. The instantaneous velocity fields, in this case, were acquired on the wake side immediately downstream of the propeller, imaging an area of about 120x90 mm. The results of this investigation are shown in Fig. 4, Fig. 5 and Fig. 6, for the angular velocities equal to 6000 RPM, 7000 RPM, and 8000 RPM, respectively, comparing the numerical predictions and the experimental measurements.

The experimental measurements and the numerical predictions show an overall good level of agreement. In particular, the streamtube dimension along the blade radial direction and its contraction as the distance from the blade increases are well captured. Only slight differences

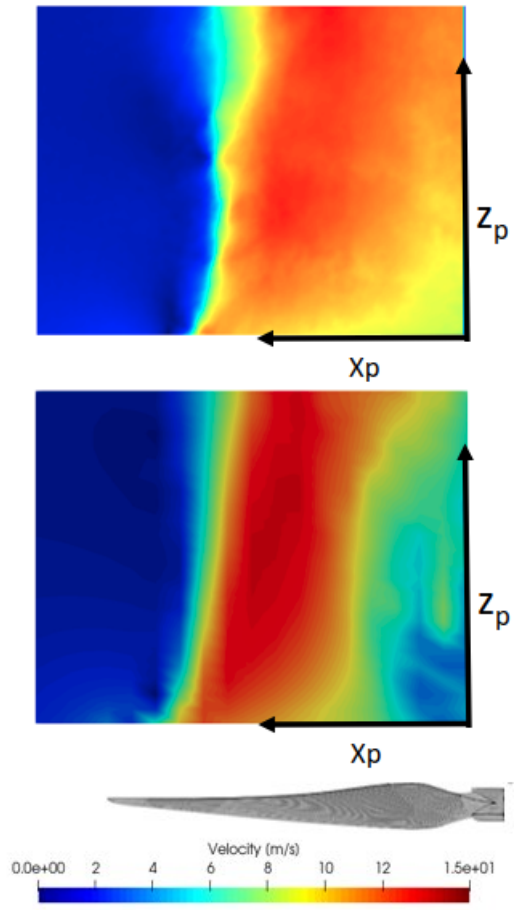

Figure 4. Comparison between the average velocity magnitude at 6000 RPM: first row experimental measurements, second row numerical results.

are observed in the middle region of the blade, where a numerical overestimation can be noticed. Major discrepancies are present in the region closer to the rotor axis, where the numerical simulations provide significantly lower velocities due to the absence of the rotor hub in the numerical setup.

4.2 Aeroacoustics

This section is addressed to the numerical/experimental correlation in terms of acoustic data. As already described, two microphones' arrays are considered as shown in Figs. 2 and 3.

The comparison between the numerical predictions

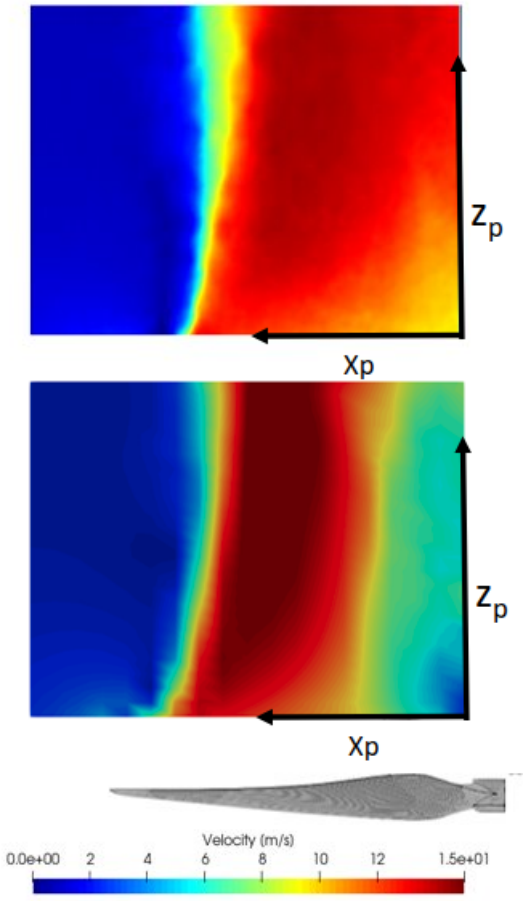

Figure 5. Comparison between the average velocity magnitude at 7000 RPM: first row experimental measurements, second row numerical results.

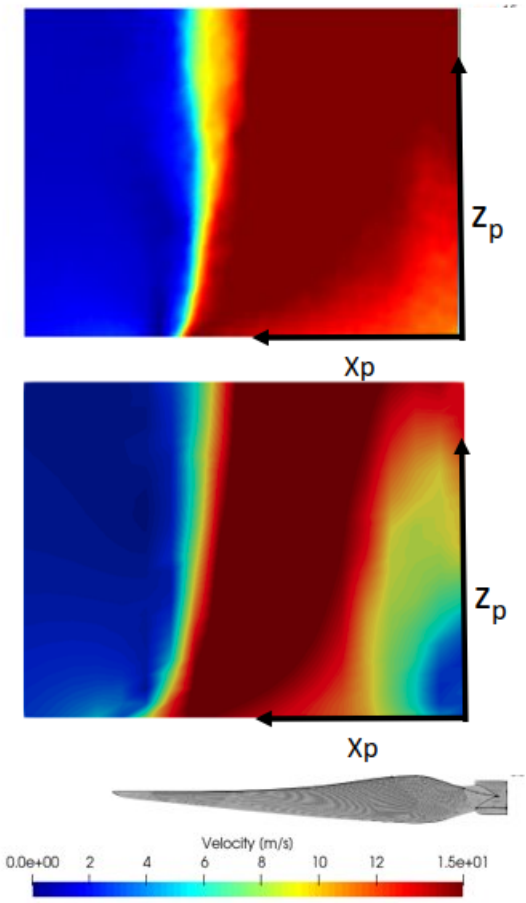

Figure 6. Comparison between the average velocity magnitude at 8000 RPM: first row experimental measurements, second row numerical results.

and the experimental measurements is shown in Fig. 7, here discussed in terms of overall sound pressure level (OASPL), evaluated by integrating the energy spectrum with respect to frequency and defined as follows:

$$OASPL = 10log_{10}\frac{\int \phi_{\text{pp}}(f)df}{p^2{}_{\text{ref}}} = 20log_{10}\frac{\sigma}{p_{\text{ref}}} \qquad (2)$$

where ϕ_{pp} is the power spectral density of the measured acoustic pressure, p_{ref} represents the reference pressure equal to 20μPa and σ indicates the standard deviation of the pressure signal, intended as the square root of the variance.

Globally, an underestimation of the emitted noise is noticeable at all the microphones investigated, with an average difference between the computation and the experiments in line with the literature available on this topic [24, 25].

First, for the azimuthal array, as expected, the numerical solver predicts an OASPL not affected by the microphone's angular position. Indeed, for the case herein investigated, namely a hovering isolated rotor, the pressure field over the propeller blades is time-invariant. On the contrary, in the experimental measurements, the OASPL shows a dependency on the polar angle. Some explanations for this unexpected behavior can be found in the presence of some asymmetries in the rotor inflow. Thus,

the directivity pattern appears to be influenced by the propeller speed exhibiting a stronger dependence when increasing the velocity.

Focusing on the polar array, the computations predict an OASPL which is higher in the rotor disk plane and then increases as the polar angle increases, regardless of the propeller angular velocity. In the overall, the experimental data show the same trend with some spurious microphones where the general trend is not respected (for instance, at 25°).

Furthermore, it is important to remind that in the numerical predictions, only the tonal contribution is captured (due to the hypothesis the numerical solver is based upon), whereas the experimental data take into account both the tonal and the broadband contributions.

5. CONCLUSION

A numerical/experimental investigation of the aerodynamics/aeroacoustics of an isolated rotor in different operative conditions has been proposed. A good agreement between the experimental measurements and the numerical predictions in terms of both flow-field and noise directivities has been observed, in line with what is found in the literature. The computations predict a velocity field that agrees well with the experimental outcomes in almost all the investigated regions, with major discrepancies in the region near to the rotor rotational axis due to the absence of the hub in the numerical simulations. Concerning the noise measurements, the numerical simulations underestimate the OASPL with respect to that experimentally measured of about 5 dB even though it strongly depends on the microphone's position, and the differences increase as the rotor angular velocity decreases. Regardless of the aforementioned differences, the good agreement between numerical and experimental results paves the way to exploit the potential of both methods to create a wide database with a reduced computational/experimental burden to be used since the early design phase of more complex innovative solutions.

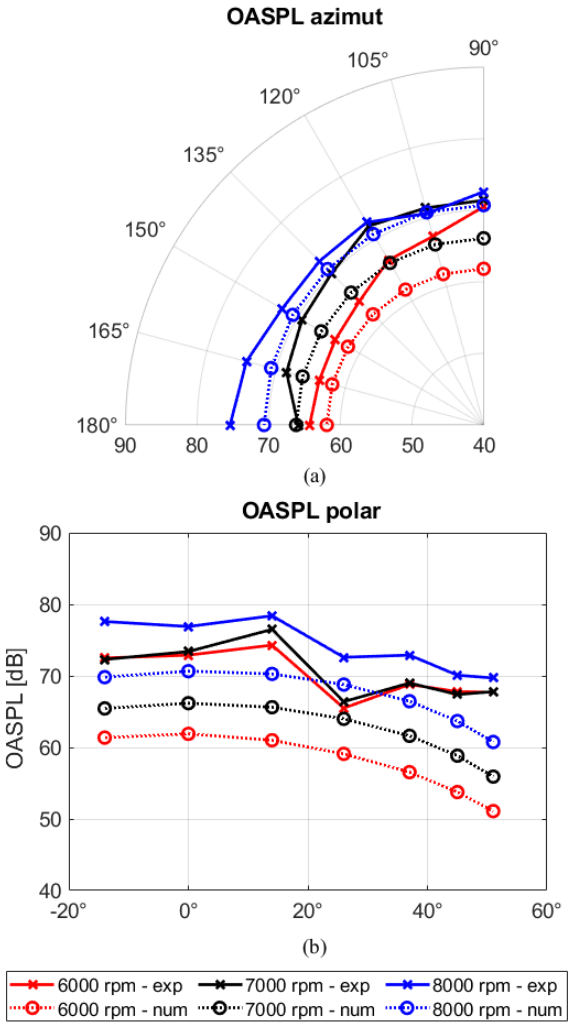

Figure 7. OASPL comparison between numerical and experimental results: first row azimuthal directivity, second row polar directivity.

6. REFERENCES

[1] EEA and EASA, *European aviation environmental report 2016*. 2016.

[2] C. Friedrich and P. A. Robertson, "Hybrid-electric propulsion for aircraft," *Journal of Aircraft*, vol. 52, no. 1, pp. 176–189, 2015.

[3] M. D. Moore, "Misconceptions of electric aircraft and their emerging aviation markets," *52nd Aerospace Sciences Meeting*, 2014.

[4] ICAO, "Guidance on the balanced approach to aircraft noise management," tech. rep., ICAO, 2008.

[5] G. Sinibaldi and L. Marino, *Experimental analysis on the noise of propellers for small UAV*. Applied Acoustics, Vol. 74, No. 1, pp. 79-88, 2013.

[6] N. Intaratep, W. N. Alexander, W. J. Devenport, S. M.

Grace, and A. Dropkin, *Experimental study of quadcopter acoustics and performance at static thrust conditions*. AIAA Paper 2016-2973, 2016.

[7] A. Leslie, K. C. Wong, and D. Auld, *Experimental analysis of the radiated noise from a small propeller*. 20th International Congress on Acoustics, 2010.

[8] C. Poggi, G. Bernardini, and M. Gennaretti, "Aeroacoustic analysis of wing-mounted propeller arrays," in *AIAA AVIATION 2021 FORUM*, p. 2236, 2021.

[9] C. Tinney and J. Sirohi, "Multirotor drone noise at static thrust," *AIAA Journal*, vol. 56, pp. 1–11, 04 2018.

[10] E. Grande, D. Ragni, F. Avallone, and D. Casalino, "Laminar separation bubble noise on a propeller operating at low reynolds numbers," *AIAA Journal*, vol. 60, no. 9, pp. 5324–5335, 2022.

[11] C. Poggi, M. Rossetti, G. Bernardini, U. Iemma, C. Andolfi, C. Milano, and M. Gennaretti, "Surrogate models for predicting noise emission and aerodynamic performance of propellers," *Aerospace Science and Technology*, vol. 125, p. 107016, 2022.

[12] C. Poggi, M. Rossetti, J. Serafini, G. Bernardini, M. Gennaretti, and U. Iemma, "Neural network meta–modelling for an efficient prediction of propeller array acoustic signature," *Aerospace Science and Technology*, vol. 130, p. 107910, 2022.

[13] T. Sinnige, R. Nederlof, and N. van Arnhem, "Aerodynamic performance of wingtip-mounted propellers in tractor and pusher configuration," in *AIAA Aviation 2021 Forum*, p. 2511, 2021.

[14] S. Gudmundsson, "General aviation aircraft design: Applied methods and procedures," *General Aviation Aircraft Design: Applied Methods and Procedures*, pp. 1–1034, 09 2013.

[15] M. Gennaretti, G. Bernardini, J. Serafini, and G. Romani, "Rotorcraft comprehensive code assessment for blade–vortex interaction conditions," *Aerospace Science and Technology*, vol. 80, pp. 232–246, 2018.

[16] M. Gennaretti and G. Bernardini, "Novel boundary integral formulation for blade-vortex interaction aerodynamics of helicopter rotors," *AIAA journal*, vol. 45, no. 6, pp. 1169–1176, 2007.

[17] M. Gennaretti, L. Luceri, and L. Morino, "A unified boundary integral methodology for aerodynamics and aeroacoustics of rotors," *Journal of Sound and Vibration*, vol. 200, no. 4, pp. 467–489, 1997.

[18] L. Morino and G. Bernardini, "Singularities in bies for the laplace equation; joukowski trailing-edge conjecture revisited," *Engineering analysis with boundary elements*, vol. 25, no. 9, pp. 805–818, 2001.

[19] G. Bernardini, J. Serafini, M. M. Colella, and M. Gennaretti, "Analysis of a structural-aerodynamic fully-coupled formulation for aeroelastic response of rotorcraft," *Aerospace Science and Technology*, vol. 29, no. 1, pp. 175–184, 2013.

[20] F. Farassat, "Derivation of formulations 1 and 1a of farassat," 2007.

[21] C. Poggi, G. Bernardini, M. Gennaretti, and R. Camussi, "Scalability of mach number effects on noise emitted by side-by-side propellers," *Applied Sciences*, vol. 12, no. 19, p. 9507, 2022.

[22] R. Camussi, M. K. Ahmad, S. Meloni, E. de Paola, and A. Di Marco, "Experimental analysis of an underexpanded jet interacting with a tangential flat plate: Flow visualizations and wall pressure statistics," *Experimental Thermal and Fluid Science*, p. 110474, 2021.

[23] E. De Paola, A. Di Marco, R. Camussi, and E. Carbini, "Aeroacoustic characterization of two pusher propellers in different configurations," *INTER-NOISE and NOISE-CON Congress and Conference Proceedings*, vol. 259, no. 3, pp. 5998–6007, 2019.

[24] A. D. Thai, E. De Paola, A. Di Marco, L. G. Stoica, R. Camussi, R. Tron, and S. M. Grace, "Experimental and computational aeroacoustic investigation of small rotor interactions in hover," *Applied Sciences*, vol. 11, no. 21, 2021.

[25] J. Yin, K.-S. Rossignol, L. Rottmann, and T. Schwarz, "Numerical investigations on small-scale rotor configurations with validation using acoustic wind tunnel data," in *48th European Rotorcraft Forum (ERF), 2022*, pp. 1–17, 2022.